Polymer 54 (2013) 258–268

Contents lists available at SciVerse ScienceDirect

Polymer

journal homepage: www.elsevier.com/locate/polymer

# Low-surface-free-energy polybenzoxazine/polyacrylonitrile fibers for biononfouling membrane

Tzu-Hao Kao [a], Jem-Kun Chen [a,*], Chih-Chia Cheng [b], Ching-Iuan Su [a], Feng-Chih Chang [b]

[a] Department of Materials Science and Engineering, National Taiwan University of Science and Technology, 43, Sec 4, Keelung Rd, Taipei 106, Taiwan, ROC
[b] Department of Applied Chemistry, National Chiao Tung University, 1001 University Road, Hsinchu 300, Taiwan, ROC

ARTICLE INFO

*Article history:*
Received 11 May 2012
Received in revised form
22 October 2012
Accepted 6 November 2012
Available online 11 November 2012

*Keywords:*
Low-surface-free-energy fibers
Polybenzoxazine
Polyacrylonitrile

ABSTRACT

We blended poly(3-phenyl-3,4-dihydro-2H-1,3-benzoxazine) (PBA) into polyacrylonitrile (PAN) to generate low-surface-free-energy fibers without fluorine and silicon elements for electrospinning. Liquid-state BA at room temperature can be solidified in electrospinning process using PAN as a medium through their miscible behavior. Results indicate that the mixing below 50 wt% BA into PAN matrix for electrospinning has no significant dropping beads, indicated a miscible PAN/BA system. Above 70 wt% BA in PAN solution could not be solidified completely after electrospinning, revealed apparent beaded fibers. The PAN/PBA blend fibers, obtained after curing at 300 °C, generated a superhydrophobicity because of the low-surface-free-energy PBA. In addition, laser scanning confocal microscope (LSCM) measurements were included to determine the relative amount of antibody that adsorbed to these PAN/PBA fibers to examine the biofouling-resistant property. The results showed an obviously decreased protein adsorption with increasing PBA fraction. The correlations between PAN and PBA would provide insight into the designing and developing of low-surface-free-energy fibers without fluorine and silicon elements to improve biofouling-resistant property.



## 1. Introduction

Superhydrophobic surfaces, which are characterized by static water contact angles higher than 150°, are divided into two classes. One is the "self-cleaning surface", which has a low sliding angle (i.e., small contact angle hysteresis). The self-cleaning surfaces have recently attracted much attention for their promising applications in various fields from daily life to industry [1]. The other superhydrophobic surface is the one with "high adhesion to water". Highly adhesive surfaces show both high water contact angle and large contact angle hysteresis. In contrast to the self-cleaning surfaces, the studies of such superhydrophobic surfaces are very limited [2]. As representative examples, a superhydrophobic polystyrene nanotube layer was aligned via template-wetting method [3], and superhydrophobic poly(propylene) surfaces with tunable sliding angles were fabricated by controlling shear and thermal conditions [4].

The fabrication or functionalization of superhydrophobic surfaces are of significant interest because of the potential utility of these nonwetting materials in a broad range of consumer, industrial, and medically oriented contexts (e.g., the design of "self-cleaning" surfaces and textiles, new nonfouling surfaces, and membranes for oil/water separation, etc.). Several methods have been used to fabricate superhydrophobic surfaces, including sol–gel processing [5], chemical vapor deposition [6], lithography [7], chemical etching [8], self-assembly [9], and electrospinning [10]. Except for the last, all of these methods are complicated and require special equipment, high temperature or vacuum conditions, or low-surface-free energy material modification involving multiple steps, which makes it difficult for practical applications in large-scale coatings. Electrospinning offers a versatile approach to fabricate unique micro and nanostructures with interesting wetting characteristics. The nanofibrous mats can be used for a broad range of applications such as filtration [11], composite materials [12], tissue engineering [13], sensor systems [14], etc.

Several approaches have been reported for combining materials of low surface energy with high surface roughness, such as electrospinning hydrophobic (PFDA-co-AA) random copolymer and polyacrylonitrile (PAN) as the second one [15] and poly[bis(2,2,2-trifluoroethoxy) phosphazene] [16] into fibrous substrates with suitable morphologies so as to make the surface superhydrophobic with or without subsequent chemical treatment. These above processes prepared superhydrophobic fibers by electrospinning certain hydrophobic polymers [17], or coating with potentially

* Corresponding author. Tel.: +886 2 27376523; fax: +886 2 27376544.
*E-mail address:* jkchen@mail.ntust.edu.tw (J.-K. Chen).

0032-3861/$ – see front matter © 2012 Elsevier Ltd. All rights reserved.
http://dx.doi.org/10.1016/j.polymer.2012.11.020

hazardous fluoro groups [18]. Polybenzoxazine (PBA) is a recently discovered class of nonfluorine, nonsilicon, low-surface-free-energy polymeric materials [19]. Benzoxazine monomer, 2,2-bis(3-methyl-3,4-dihydro-2H-1,3-benzoxazinyl)propane, can be used to produce polybenzoxazine films by spin-coating and curing in an oven. The surface free energy of polybenzoxazine film is 16.4 mJ/m$^2$, which is even lower than that of PTFE by 21 mJ/m$^2$ [20,21]. Polybenzoxazine rarely dissolves in the solvent to manufacture as fibrous structure because of its cross-linking chains. In general, the BA can be used as a precursor to obtain polybenzoxazine films after curing. However, when BA liquid (solution) is drawn out of the tip of a nozzle, it cannot transform into a minuscule fiber upon drying or solidifying and form a nonwoven fabric on a collective target. Therefore, the practical applications of polybenzoxazine for electrospun super-hydrophobic mats are significantly limited. For improving the polybenzoxazine practical application of fibrous mats, PAN is an ideal blend material due to its high melting temperature [22]. In this study, we demonstrate a facile fabrication of a nonfluorine, nonsilicon fabric from electrospun fibers comprising of PAN and PBA, which is one of low surface energy polymers. Precursor fibers of PAN/BA hybrids with various BA fractions are generated by electrospinning. After curing PAN/BA hybrid fibers, PAN/PBA blend fibers can be obtained. To the best of our knowledge, this paper is the first report of an electrospun mat exhibiting a low surface energy without fluorine and silicon elements. These fibrous structures can be applied in diverse applications, including self-cleaning glasses and clothes, protection against corrosion of metallic parts, antiprotein adsorption and antisnow sticking.

## 2. Experimental section

### 2.1. Materials

Polyacrylonitrile (PAN) (Aldrich Co) with an average molecular weight (Mw) of 150.000 g/mol was used as received. Paraformaldehyde (Aldrich, 95%), phenol (Aldrich, 99.5%), aniline (Aldrich, 99.5%), and dimethylformamide (DMF) were used without further purification. Aniline (Acros, 99.5%) was distilled before use. N,N-Dimethylformamide (DMF) (Aldrich, 99.8%) were utilized as received. 3-phenyl-3,4-dihydro-2H-1,3-benzoxazine (BA) was synthesized and purified according to the procedure described elsewhere [23]. The synthesized BA was purified by dissolving in the 1 L diethyl ether, and washing three times with 1.5 L of aqueous 3 N sodium hydroxide, and finally five times with 1 L distilled water. The ether solution was dried with anhydrous sodium sulfate followed by evaporation of ether under vacuum to afford pale yellow liquid.

### 2.2. Preparation of electrospun PAN/PBA fibrous mats

The DMF solution with 10 wt% PAN was stirred for 1 h before use. Binary mixture experiments between BA and PAN were performed in DMF at increasing BA to PAN weight ratios: 0, 30, 50, 70 and 100 wt%. Dispersions of BA were added dropwise into PAN solution, and were stirred for 1 h at room temperature. The solution was filtered through a 0.2 μm syringe before both of electrospinning and spin-coating. The PAN:BA weight ratios for the various hybrids were 100:0, 70:30, 50:50, 30:70 and 100:0 in DMF solutions, denoted as P10B0, P7B3, P50B50, P3B7 and P0B10, respectively. The concentration of the PAN/BA hybrids in DMF solution was controlled at 10 wt% for P10B0, P7B3, P50B50, P3B7 and P0B10. For electrospinning, a syringe pump (KDS-100, KD Scientific. Co., Ltd.) was fixed to a support which could be moved rightward and leftward with a speed of 7 m/min along a slipway to jet the PAN/BA hybrid solution uniformly on a rolled cylinder substrate as films. The metal needle tips of the syringes were connected to the positive electrode of a high voltage power supply (YSTC Technology Co.). The feeding rate of polymer solutions was 1 mL/h. The applied voltage was 20 kV, and the tip-to-collector distance was 15 cm. The fibrous mats were collected on the surface of aluminum foil and dried at room temperature in vacuum for 24 h prior to the subsequent characterizations. The PAN/BA hybrid fibers involving P10B0, P7B3, P5B5, P3B7 and P0B10 were cured at 300 °C for 2 h under nitrogen environment to obtain poly(3-phenyl-3,4-dihydro-2H-1,3-benzoxazine) (PBA) blending with PAN as fibrous mats, denoted as P10PB0, P7PB3, P5PB5, P3PBA7 and P0PB10, respectively. In addition, the PAN/BA hybrid solutions were spin-coated onto a glass by immediate spinning at 1500 rpm for 30 s; they were then cured at 300 °C for 2 h under vacuum to obtain the PAN/PBA coating for comparison.

### 2.3. Miscibility and curing behavior of the PAN/BA hybrids

The PAN/BA hybrids were analyzed by Fourier transform infrared spectroscopy (FTIR) to assess their effects on thermal property. All spectra collected using FTIR of the PAN/BA hybrids were recorded using the KBr disk method. The FTIR spectra were recorded with a 8 cm$^{-1}$ spectral resolution and degassed with nitrogen on a Digilab FTS-1000. A total of 20 scans were accumulated for signal-averaging of each IR spectral measurement to ensure a high signal-to-noise ratio. Peaks at δOH free, δOH intra HB, δOH inter HB, νNH inter HB, νNH intra HB, νN$^+$H intra HB were adopted to evaluate the interactions of PAN/BA and PAN/PBA systems by the de-convolution procedure (fitting function). The samples were further cured at 300 °C for 2 h to identify the formation of PAN/PBA blending by FTIR. Differential Scanning Calorimetry (DSC) analyses were performed on a Perkin Elmer (DSC 4000) in the range of 30–300 °C with heating rate of 10 °C/min under nitrogen flow to determine the curing temperature (Tc) of BA and degradation temperature (Td) of PAN, respectively. Approximately 5–10 mg sample was weighed and sealed in an aluminum pan. The sample was then quickly cooled to room temperature from the first scan and then scanned between 30 and 300 °C at a scan rate of 5 °C/min. Tc and Td were taken as the midpoint of the exothermal peaks.

### 2.4. Characterization and non-biofouling of the PAN/PBA fibrous mats

PAN/BA hybrid and PAN/PBA blend fibrous mats were observed through a field-emission scanning electron microscopy (FE-SEM) (JEOL, JSM 6500F) operating at 15 kV after platinum coating. The diameters of fibers were measured using image analysis software (Image-Pro plus). Static water contact angle (SWCA) measurements were performed by increasing the drop volume and recording the angle on a GH-100 Contact Angle System (KRÜSS GmbH LTD.). The SWCA was determined by fitting a Young–Laplace curve around the drop. The experiment was performed under normal laboratory ambient conditions, 35% relative humidity. The mean value was calculated from at least 10 individual measurements and the measurement error was less than 3°. In addition, it is well known that a heterogeneous surface (chemically or geometrically) usually shows contact angle hysteresis [24]. That is, for a geometrically rough surface, contact angle hysteresis originates primarily from the rough contact interface that depends upon the contact area of water with the structured surface. The earliest work to model liquid drops on a roughness surface can be contributed to Wenzel [25] and Cassie [26]. Their models are described by the following equations.

$$\cos\theta_r = r\cos\theta_s \quad (1)$$

$$\cos\theta_r = f_1\cos\theta_s - f_2 \quad (2)$$

where $\theta_r$ and $\theta_s$ are the equilibrium (Young's) SWCA of a rough surface and a smooth surface, respectively. $f_1$ and $f_2$ are the fractions of a solid surface and air in contact with a liquid droplet, respectively ($f_1 + f_2 = 1$). The Equation (2) assumes that a liquid does not completely wet a rough surface. Once air is trapped in the interstices of a rough surface, a liquid droplet interacts with the composite surface that consists of a solid substrate and air pockets. It is well understood that there is no unique contact angle to characterize any given surface. The observed equilibrium contact angles always fall between the advancing and receding contact angles. The contact angle hysteresis $\Delta\theta$, defined as the difference between advancing and receding contact angles ($\Delta\theta = \theta_{adv} - \theta_{rec}$), can be used to conclude the state of a liquid droplet.

In the Wenzel state, the textured surface has a higher effective surface area than does a smooth surface. The water droplet completely penetrates the surface texture and wets a smaller apparent area, resulting in a higher SWCA compared to that on a smooth surface. However, as predicted by Equation (1), this SWCA enhancement occurs only for hydrophobic materials that have a $\theta_s > 90$ on a smooth surface. For $\theta_s < 90$, surface roughness makes the material more hydrophilic. Although the Wenzel state can result in enhanced SWCA, it is not preferred for many applications because it has very high (wetting/dewetting) hysteresis and pinning behavior on the substrate. In the Cassie–Baxter state, the droplet does not make continuous contact with the solid surface. Instead, the water droplet sits on the composite surface of trapped air and solid. This composite surface has a higher SWCA because of the air/liquid interface and can result in superhydrophobicity. The Cassie–Baxter state is preferred because of very small hysteresis and excellent rolling behavior even at tilt angles of a few degrees. This implies that the contact angle hysteresis is responsible for the pinning of liquid droplets on a surface.

To evaluate the low-surface-free-energy property of the fibers, PAN/BA hybrid and PAN/PBA blend fibers were examined by a biofouling experiment. The distribution and biofouling of the protein adhered on the fiber surfaces were investigated by the laser scanning confocal microscope (LSCM; Leica TCS SP5 Confocal Spectral Microscope Imaging System) technology through 100 mW Ar blue Laser with 488 nm wavelength. Antibodies, fluorescein (FTIC)-conjugated AffiniPure Goat Anti-Rabbit lgG (H + L), code number: 111-095-003, purchased from Jackson Immuno Research Laboratories, INC, was used in the study. This is in contrast to viable antibodies that are only adhered on the fibers and produce green fluorescence. In the experiments, the fibers were immersed into the FTIC-conjugated antibody solution for 12 h. The antibody-adhered fibers were subsequently observed by the LSCM through their fluorescence.

## 3. Results and discussion

FTIR measurements were used to calculate the fraction of hydrogen bonding in the hybrids, a highly effective method of quantitative analysis of the specific interactions between macromolecules. Fig. 1 represents the vibrational spectra of PAN/BA hybrids for P10B0, P7B3, P5B5, P3A7 and P0B10 before thermal treatment. In a film of neat PAN, two major absorption bands for the PAN show the characteristic bands, such as those at absorption bands are observed around 2243–2240 and 2928 $cm^{-1}$, attributed to the C≡N stretches and the C–H stretches of the sp3 carbons [27]. For the pure BA, the characteristic absorptions of BA structure

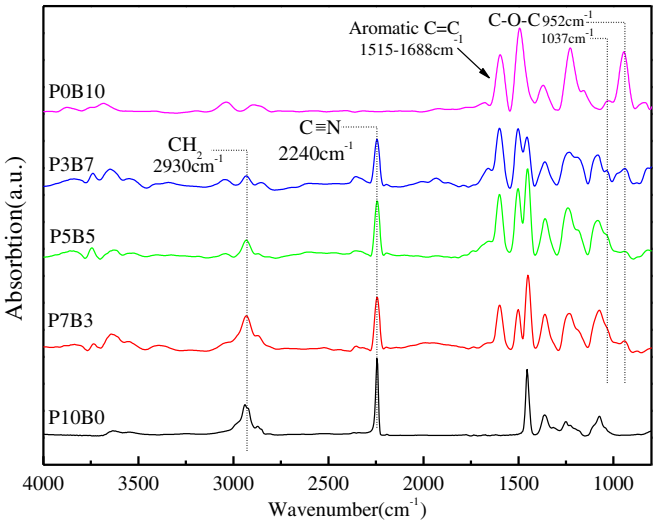


**Fig. 1.** FTIR spectra of PAN/BA hybrids before curing for P10B0, P7B3, P5B5, P3B7 and P0B10.

appear at 1230–1236 $cm^{-1}$ (asymmetric stretching of C–O–C), at 1028–1036 $cm^{-1}$ (symmetric stretching of C–O–C), and at 1327–1340 $cm^{-1}$ ($CH^2$ wagging) [23]. The broad band from 952 to 1037 $cm^{-1}$ is attributed to C–O–C (vibrational mode of cyclic and symmetric stretching) in plane deformation modes of BA. Moreover, the band observed at 1454 $cm^{-1}$ corresponds to C–N ring stretching vibration of BA. In the presence of BA, an increase was observed in this absorbance of 1454 $cm^{-1}$ by introducing BA in the PAN matrix.

The miscibility and curing behavior of the hybrids along with the typical BA was examined by means of DSC. The uncured hybrids were subjected to thermal analysis and the conventional first run DSC thermograms of the PAN/BA hybrids for P10B0, P7B3, P5B5, P3B7 and P0B10 are shown in Fig. 2. A sharp exotherm at ca. 290 °C is observed for P10B0 corresponding to the secondary stabilization (Fig. 2a). Various reaction schemes have been proposed to occur during stabilization. Houtz [28] suggested the formation of a heteroaromatic, cyclic structure. Later workers [29–31] have favored a cyclic polyimine structure frequently referred to as "ladder polymer" (Scheme 1). The sharp exotherm of PAN shifted to lower a temperature upon hybridizing the BA in the PAN; that is, it shifted from 290 °C to 275 °C for P7PB3 (Fig. 2b). For P5B5, the sharp exotherm turned to a blunt one, which the onset and maximum temperatures of the exotherm were at 202 and 230 °C, respectively. With addition of BA in PAN to 50 wt%, only one exotherm is detected by DSC for both of P7B3 and P5B5 (Fig. 2b, c). As seen in Fig. 2e, a single exothermic peak appeared at ca. 237 °C for P0B10 (pure BA) indicates the ring-opining temperature (Tc) of BA. For a hybrid of macromolecules, a single peak detected by DSC is conventionally employed as a criterion reflecting the miscibility of the hybrid. The results exhibit that the significant miscibility of the PAN/BA hybrids occurred below 50 wt% BA in the PAN, indicated that BA could be dissolved completely in PAN phase upon 50 wt% concentration. However, two peaks appeared at ca. 200 and 300 °C for P3B7 indicate that the phase separation between BA and PAN occurs at 70 wt% BA content, indicating a saturation content of BA in the PAN (Fig. 2d). Even the phase separation occurs in the hybrids, the interaction between PAN and BA leads to the acceleration of the curing reaction of the BA and degradation of PAN, shifting both of the exotherm peaks to lower temperature. Furthermore, the area under the exothermal peaks increased from 336 J/g for the pure BA to 558 J/g for P5B5, but decreased to 540 J/g for P7B3. The P5B5

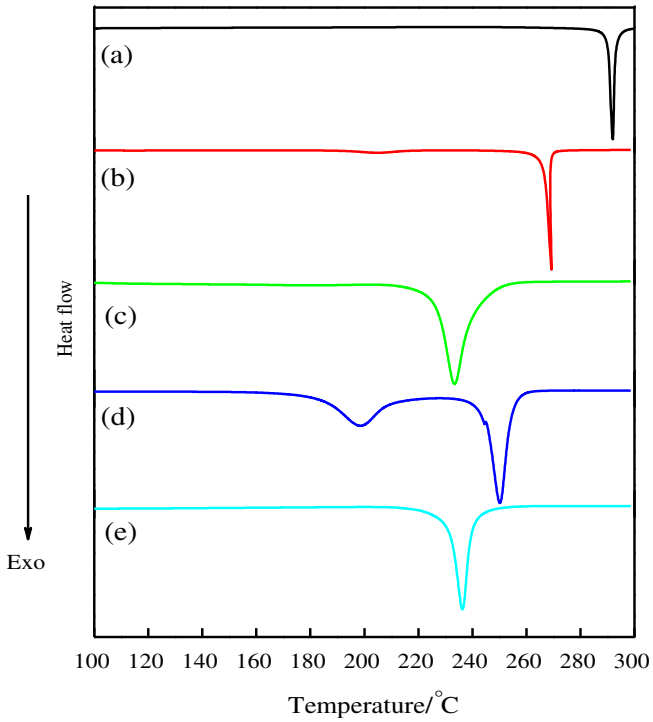


**Fig. 2.** Conventional first run DSC thermograms of the PAN/BA hybrids including (a) P10B0, (b) P7B3, (c) P5B5, (d) P3B7 and (e) P0B10, respectively.

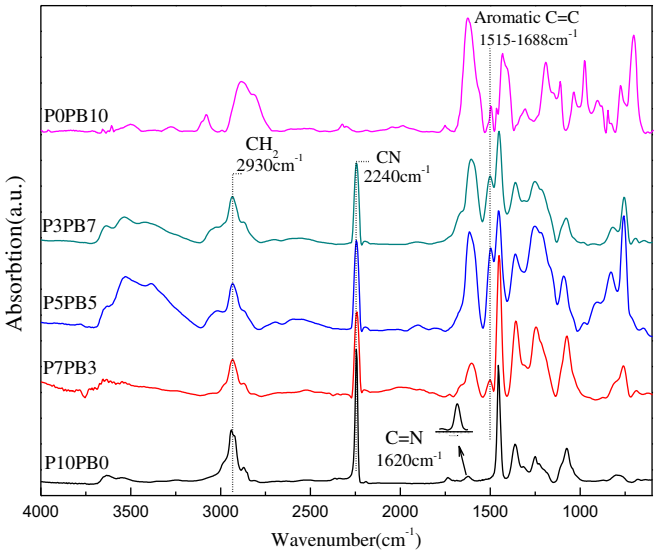


**Fig. 3.** FTIR spectra of PAN/PBA blends after curing for P10PB0, P7PB3, P5PB5, P3PB7 and P0PB10.

hybrid exhibits the largest exotherm of these hybrids during the thermal treatment. This observation suggests that only a certain fraction of the binary mixtures contributed to the significantly exothermic network formation reaction in the binary hybrid.

Thermally activated ring-opening of BA affords the PBA networks which bear a great amount of phenolic hydroxyl groups (Scheme 1). In addition, PAN is stabilized by heating in air at temperatures in the range 200 °C–300 °C. These phenolic hydroxyl groups of PBA interact with the hydrogen bonding to the heteroaromatic or polyimine cyclic structure occurred during stabilization of PAN, which are readily investigated by means of FTIR. Fig. 3 represents the PAN/PBA blends of FTIR spectra for P10PB0, P7PB3, P5PB5, P3PB7 and P0PB10 after thermal curing at 300 °C for 2 h. In the IR spectra of P0PB10, the characteristic absorption bands due to BA structure at 952 $cm^{-1}$ (vibrational mode of cyclic C–O–C), at 1037 $cm^{-1}$ (symmetric stretching of C–O–C), and at 1348 $cm^{-1}$ ($CH_2$ wagging) disappeared after the 300 °C cure, suggesting the completion of ring-opening of BA to afford PBA. The bands in this region are assignable to the stretching vibration of phenolic hydroxyl groups. A broad band centered at 3437 $cm^{-1}$ is ascribed to the stretching vibration of hydrogen bonded phenolic hydroxyl groups [30]. A single peak at 3120 $cm^{-1}$ band of the neat PBA, ascribed to the hydrogen bonded phenolic hydroxyl groups, disappeared for P7PB3, P5PB5 and P3PB7, it may shift to 3200–3300 $cm^{-1}$ overlapping other peaks of hydrogen bonding for the PAN/PBA systems. Furthermore, a new band for the tetrasubstituted aromatic ring of the polymerized BA appears at 1480 $cm^{-1}$, with a corresponding decrease in the intensity of the band, representing the trisubstituted aromatic ring of PBA (1498 $cm^{-1}$). For P10PB0, the changes in the IR spectra are consistent with those observed in other studies [19,29]. In addition, acrylonitrile unit in the polymer chain at 2243–2240 $cm^{-1}$ (stretching C≡N), at 1680 $cm^{-1}$ (C═N), 3390 $cm^{-1}$ ($NH_2$), 3230 $cm^{-1}$ (NH) and the bands in the regions 2931–2870, 1460–1450, 1380–1350, and

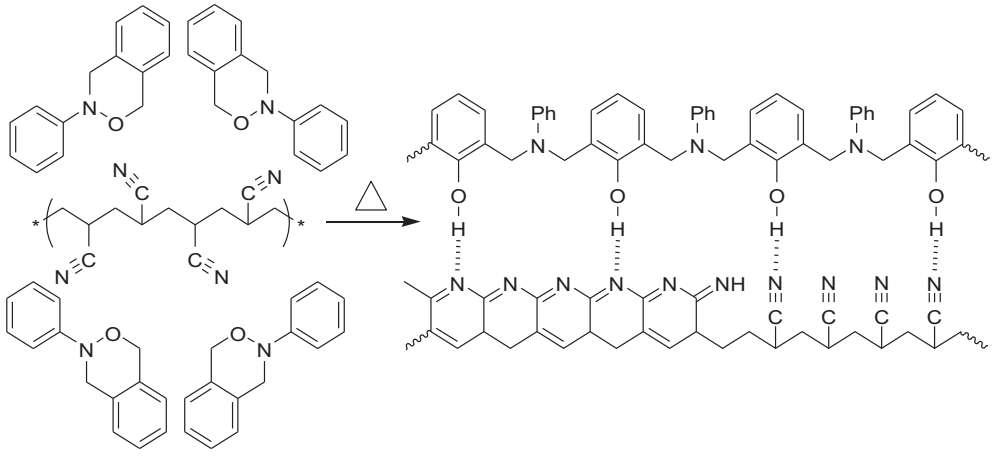


**Scheme 1.** Intermolecular hydrogen bonding between hydroxyl groups of PBA chains and heteroaromatic or polyimine cyclic groups presented in the PAN after curing PAN/BA hybrids.

1270–1220 $cm^{-1}$ which are assigned to the aliphatic CH group vibrations of different modes in CH and $CH_2$. The nitrile band at 2240 $cm^{-1}$ is reduced partially, ascribed to residual nitrile absorption. A broad band with a maximum at about 3400 $cm^{-1}$ and a shoulder at 3200–3300 $cm^{-1}$ appears suggesting a –NH structure, possibly an imine C═NH. An intense doublet also appears with maxima at 1610 and 1580 $cm^{-1}$. The former is consistent with conjugation, either $-(C{=}C)_n-$ or $-(C{=}N)_n-$; the latter is likely to be caused by the –NH structure. Further intense bands occur at 1380, 1250 and 1150 $cm^{-1}$ which completely mask the original bands between 1000 and 1500 $cm^{-1}$. Fig. 4a–e displays expanded FTIR spectra in the range of 4000–2000 $cm^{-1}$ for P10PB0, P7PB3, P5PB5, P3PB7 and P0PB10 with corresponding curve fitting. Three different kinds of OH groups and two different kinds of NH group present in the PAN/PBA mixtures: free OH groups (ca. 3630 $cm^{-1}$), OH···N intramolecular hydrogen bonds (ca. 3200 $cm^{-1}$), OH···O intermolecular hydrogen bonds (ca. 3420 $cm^{-1}$), NH··· N multiple intermolecular hydrogen bonds (ca. 3380 $cm^{-1}$), and NH···O

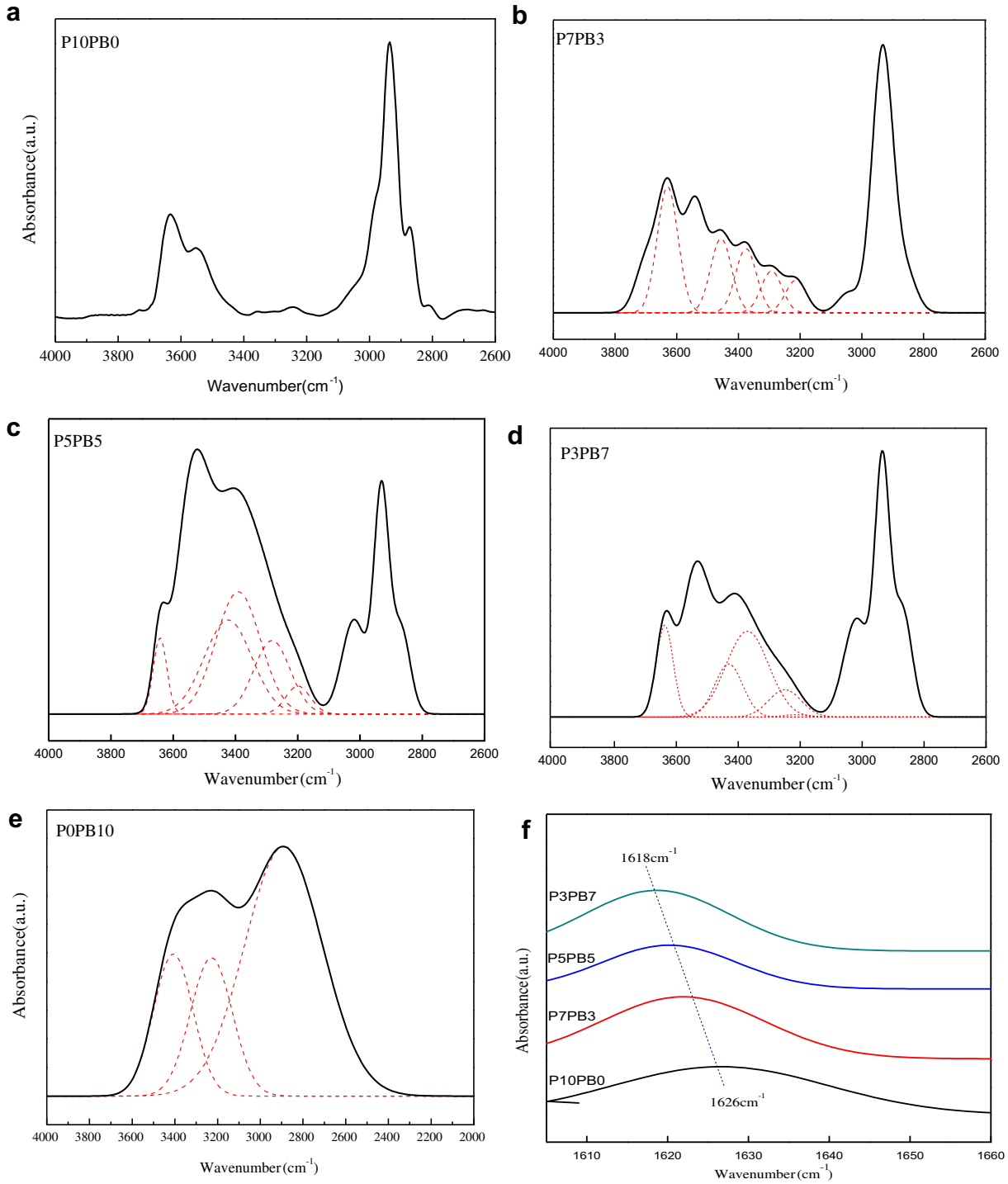


**Fig. 4.** Expanded FTIR spectra in the range of 4000–2000 $cm^{-1}$ for (a) P10PB0, (b) P7PB3, (c) P5PB5, (d) P3PB7 and (e) P0PB10 with corresponding curve fitting, and (f) at the C═N stretching band region of PAN/PBA blends for P10PB0, P7PB3, P5PB5, P3PB7 and P0PB10 at room temperature.

intermolecular hydrogen bonds (ca. 3240 $cm^{-1}$), consistent with our assignment in Scheme 1. For the PAN/PBA blends, two different kinds of hydrogen bonds were evident (Fig. 4b–d): OH···O intramolecular hydrogen bonds (ca. 3170 $cm^{-1}$) [19], OH···N intermolecular hydrogen bonds (ca. 3250–3420 $cm^{-1}$). The OH···O intramolecular hydrogen bonds of PBA at 3170 $cm^{-1}$ shifts to 3100 $cm^{-1}$ because of the binary mixtures. The broad band in the range of 3200–3600 $cm^{-1}$ increased apparently, verifying that the intermolecular hydrogen bonding between PAN and PBA occurred. Area of the broad band of the P5PB5 blend approaches a maximum, indicating that the strongest intermolecular hydrogen bonding between PAN and PBA occurred at the 50 wt% concentration PBA blending with PAN. These results indicate that intramolecular hydrogen bonding of PBA transferred substantially to intermolecular hydrogen bonding with PAN. In addition, a clear shift of PAN at 1620 $cm^{-1}$ was observed arising from the protons on the –(C═N)$_n$–of PAN to –OH (C═N···H–O) of PBA, verifying the deprotection of PBA (Fig. 4f). We summarize the deconvolution data (positions and relative areas of the components) obtained for relevant regions in the FTIR Spectra of PAN/BA hybrids and PAN/PBA blends in Table 1.

Using the binary mixture solution, its flow rate needs to be limited to ≤1 mL/h to prevent dripping problems. However, when a pure BA solution is used for electrospinning, dripping problem is extremely apparent because liquid state BA could not be solidified at room temperature. PBA is rarely dissolved in most of solvents at room temperature for electrospinning. Therefore, PAN is regarded as a medium to electrospun BA through their miscibility. Top-view SEM (left) and side-view SEM images (45° oblique angle; right) of electrospun PAN/BA hybrid fibers are shown in Fig. 5. The fractions of the BA in the PAN solution had a marked effect on the fiber diameter and morphology. The fiber diameter of the electrospun by pure PAN fiber is ca. 456 ± 97.2 nm (Fig. 5a) Using PAN/BA hybrid solution results in larger fiber diameters upon 50 wt% BA content, indicated that liquid state BA substantially extended the diameter of the electrospun fibers (Fig. 5b, c). For P3B7, the beaded fiber appeared significantly, and the fiber diameter abruptly increases to ca. 1144 nm since a large fraction of BA did not be solidified after electrospinning (Fig. 5d). It is well known that thinner fiber diameters and higher bead densities improve the superhydrophobicity [32]. However, in practical applications, dripped fibers are not desirable because of their poor mechanical properties. After curing at 300 °C for 2 h, PAN/PBA blend fibrous mats are observed by top-view SEM (left) and side-view SEM images (45° oblique angle; right) as shown in Fig. 6. Comparing with the side-view SEM images (45° oblique angle) of the surface before curing, it is found that the fiber mat seems to slightly collapse on the surface because of the flexible nature of the polymer at high temperature [18]. The diameter of PAN/PBA blend fibers decrease slightly after curing the BA in the fiber, attributed to the excess solvent removing and the formation of PBA. We summarize these data of the PAN/BA hybrid and PAN/PBA blend fibers in Table 2.

The static water contact angle (SWCA) and hysteresis measurements are considered to be important to examine the surface hydrophobicity. The wettability of the various surfaces was estimated by measuring the contact angles of water droplets on these surfaces prepared by spin-coating and electrospunning for PAN/BA hybrids as shown in Fig. 7a. Generally, it is believed for hydrophobic materials that the rough surface has a higher hydrophobicity than the flat surface [33]. The water droplet on spin-coated and electrospun PAN fibrous mats apparently exhibits SWCA of 44 ± 3° (hydrophilic) and 104 ± 3°(hydrophobic), respectively, showing apparently that the SWCAs of surfaces prepared by electrospinning are larger than that by spin-coating. SWCAs of the spin-coated PAN/BA hybrid surface increases gradually with the BA fraction, indicating the BA in the hybrids substantially enhances the hydrophobicity. As we expected, the fiber structure enhances the hydrophobicity on the surface. For the PAN/BA hybrid fibrous mats, the SWCA increased from 104 ± 3° to 120 ± 3° upon increasing BA content to 50 wt%. For the P3B7, the SWCA of the surface decreased abruptly to 115 ± 3° because of the beaded fiber structure. The value of 120° indicated that the surface was highly hydrophobic, but did not meet the criterion of superhydrophobicity (SWCA higher than 150°). After curing the PAN/BA hybrid fibers, all SWCAs of PAN/PBA blend fibrous mats increase significantly (Fig. 7b) The PAN/PBA fibrous mats for P5PB5 exhibited the largest SWCA of 154 ± 3°, indicative of superhydrophobicity. The hydrophobicity of the fibrous mats is ascribed to the air trapped between fibers and surface chemistry. The trapped air can prevent the intrusion of water into the nanostructures, resulting in increase of the water contact angle on the fiber surface. On electrospun fiber mats, the water droplet is either in the Cassie–Baxter state or the metastable Cassie–Baxter state, and the SWCA is increased as a result of surface roughness and entrapped air within the fibers. This explanation could be confirmed by the Equation (2) proposed by Cassie and Baxter [25,26]. The Equation (2) assumes that a liquid does not completely wet a rough surface. Once air is trapped in the interstices of a rough surface, a liquid droplet interacts with the composite surface that consists of a solid substrate and air pockets. From the Equation (2), a very hydrophobic surface is realized if air fraction is large enough. For the PAN/BA hybrid surface, air fraction was calculated to be in the range of 0.524–0.63 upon 50 wt% of BA content (Table 1). For P3B7, air fraction was ca. 0.31 consistent with the observation of SEM images. The thermal treatment process collapsed slightly the hybrid fiber layer, but raised all air fractions of the fibrous mats.

**Table 1**
Deconvolution data (positions and relative areas of the components) obtained for relevant regions in the FTIR spectra of PAN/BA hybrids and PAN/PBA blends.

| Sample no. | Wavenumber, $cm^{-1}$ (area %)[a] | | | | | |
|---|---|---|---|---|---|---|
| | δOH free[b] | δOH intra HB | δOH inter HB | νNH inter HB[c] | νNH intra HB[d] | $\nu N^{+}H$ intra HB |
| P7B3 | 3635 (2.1) | 3214 (7.8) | 3408 (4.1) | 3227 (1.5) | 3359 (4.2) | |
| P5B5 | 3635 (0.3) | 3187 (1.8) | 3404 (7.2) | 3257 (0.1) | 3360 (10.2) | |
| P3B7 | 3648 (2.3) | 3203 (0.1) | 3421 (0.5) | 3243 (0.2) | 3369 (0.8) | |
| P0B10 | | 3203 (0.2) | 3422 (0.1) | | | 2762 (5.5) |
| P7PB3 | 3629 (2.6) | 3214 (2.1) | 3429 (2.4) | 3240 (6.9) | 3375 (11.7) | |
| P5PB5 | 3642 (3.1) | 3199 (2.1) | 3423 (9.1) | 3245 (8.0) | 3370 (9.2) | |
| P3PB7 | 3637 (4.1) | 3211 (0.1) | 3430 (3.9) | 3249 (2.3) | 3370 (9.7) | |
| P0PB10 | | 3229 (9.7) | 3425 (8.7) | | | 2755 (10.5) |

[a] Peak wavenumber.
[b] Free: non-hydrogen bonded.
[c] Inter HB: intermolecular hydrogen bonded.
[d] Intra HB: intramolecular hydrogen bonded.

From the SWCAs on the P5PB5 surface, air fraction was calculated to be 0.86, indicating that about 86% of the PAN/PBA surface was occupied by air. Air fraction was calculated to be 0.336 on the P3PB7 surface close to that on the P3B7 surface, illustrated that the decrease of the air fraction consistent with the observation of their SEM images. Therefore, hydrophobicity of the fibrous mats is believed to be mainly caused by the trapped air between the fibers, and the PBA content in the fibers.

The sliding behavior of a water droplet is mainly related to contact angle hysteresis, which is defined as the difference between advancing and receding contact angles, and continuity of three-phase (solid–liquid–air) contact line [34]. On most of flat surfaces, a water droplet comes to rest at a local energy minimum due to either chemical structures or topography, and the three-phase contact line is fixed. Therefore, there are energy barriers for advancing and receding movements of a water droplet, which cause contact angle hysteresis. Therefore, there are energy barriers for advancing and receding movements of a water droplet, which cause contact angle hysteresis. The energy barriers can be large if the contorted, continuous contact line with a water droplet is

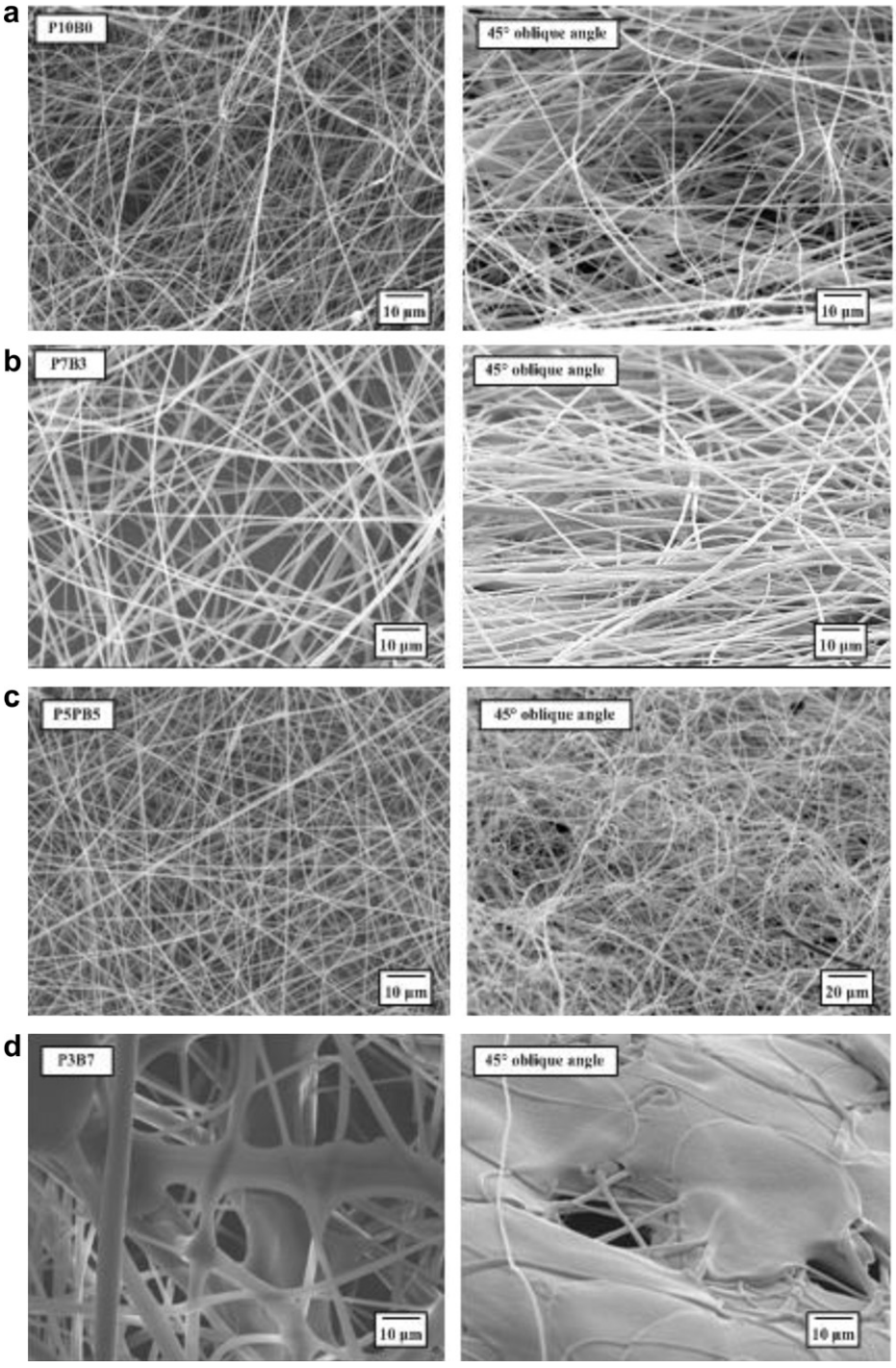


**Fig. 5.** Top-view SEM (left) and side-view SEM images (45° oblique angle; right) of electrospun PAN/BA hybrid fibers for (a) P10B0, (b) P7B3, (c) P5B5, and (d) P3B7, respectively.

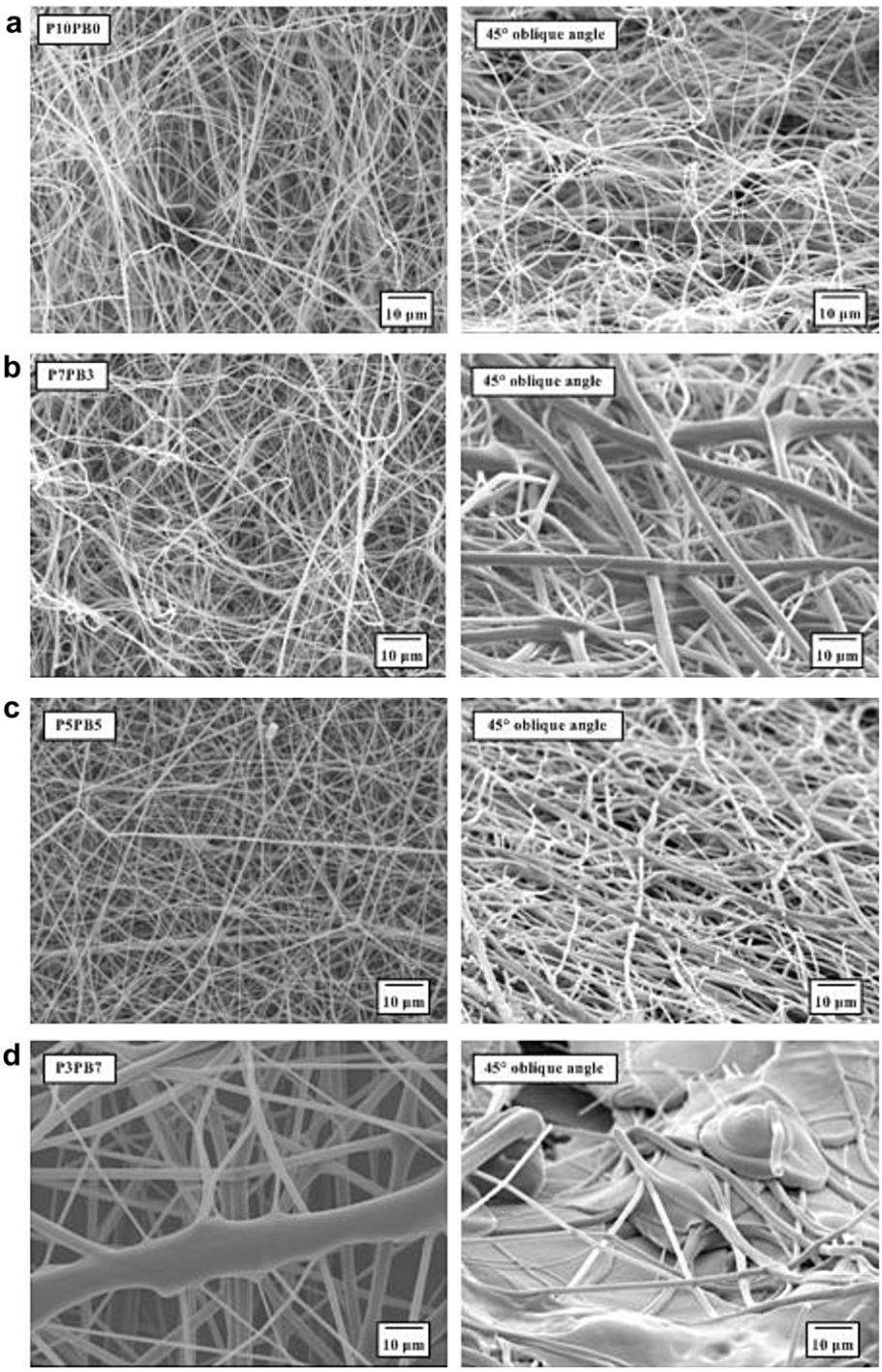


**Fig. 6.** Top-view SEM (left) and side-view SEM images (45° oblique angle; right) of electrospun PAN/PBA blend fibers for (a) P10PB0, (b) P7PB3, (c) P5PB5, and (d) P3PB7, respectively.

formed, inducing a water droplet which does not move easily on the surface [35]. Based on the FE-SEM images of the PAN/PBA fibrous mats shown in Fig. 6, the three-phase contact line was continuous on the surface. The continuous contact line, causing drops do not move spontaneously or easily on these surfaces. As we expected, a water droplet did not slide on the PAN/PBA nanofibrous surface, even when the surface was tilted at 90° (left) or turned upside down (right) as shown in Fig. 8. The fibrous surface could hold 2 μL of a water droplet at maximum with 90°-tilting, indicating strong adhesion between water and the surface. The strong adhesion between polar water and PAN/PBA fibrous structures can be explained mainly by the interaction caused by hydrogen bonding [36]. This explanation can be explained by that each PAN/PBA fiber generates low surface energy, but lots of fibers collectively create the formidable adhesion [37]. The effect of the PAN/PBA blend fibrous mat for P5PB5 is similar to a bio-mimic surface. The mechanism of the bio-mimic surface suggests that the remarkable adhesion property of the bio-mimic surface is mainly the result of the size and shape of the fibers, and is also strongly affected by low-surface-free-energy property of the surface. Therefore, the densely-

**Table 2**
Fiber diameter, SWCAs, hysteresis, and fractional interfacial areas of solid and air contact with a water droplet ($f_1$ and $f_2$) for PAN/BA hybrids and PAN/PBA blend fiber mats prepared by electrospinning and spin-coating, respectively.

| Sample | Fiber diameter (nm) | SWCA (deg) | | Hysteresis[a] | | Fractions of the fibers contact with a water droplet ($f_1$)[b] | Fractions of air contact with a water droplet ($f_2$)[b] |
|---|---|---|---|---|---|---|---|
| | | Spin-coating | Electrospinning | Spin-coating | Electrospinning | | |
| P10B0 | 456 ± 97.2 | 44 ± 3° | 100.5 ± 3° | 6° | 16° | 0.475 | 0.524 |
| P7B3 | 478 ± 152.3 | 55.8 ± 3° | 110 ± 2° | 11° | 40° | 0.421 | 0.578 |
| P5B5 | 494 ± 72.7 | 69.4 ± 2° | 120 ± 2° | 11° | 34° | 0.369 | 0.63 |
| P3B7 | 1144 ± 173.1 | 83.5 ± 3° | 104 ± 3° | 12° | 2° | 0.68 | 0.31 |
| P10PB0 | 430 ± 95.2 | 49 ± 3° | 108.3 ± 3° | 15° | 31° | 0.291 | 0.709 |
| P7PB3 | 466 ± 77.9 | 68.2 ± 3° | 120 ± 2° | 19° | 20° | 0.261 | 0.738 |
| P5PB5 | 482 ± 74.0 | 88.3 ± 2° | 154 ± 2° | 18° | 16° | 0.13 | 0.86 |
| P3PB7 | 1130 ± 280.932 | 93.2 ± 3° | 112 ± 3° | 22° | 1° | 0.663 | 0.336 |

[a] Difference between advancing and receding contact angles.
[b] Calculated by Equations (1) and (2).

packed fibrous structure of the P5PB5 surface in our system is the key contributor to the enhancement of hydrogen bonds, giving high adhesion between water and the low surface energy mat [38]. As seen in Fig. 8, for all four number ratio of PAN/PBA fibrous, such as P10PB0, P7PB3, P5PB5 and P3PB7 also had the high adhesion forces of fibrous mats even when the surfaces were tilted. Therefore, we believe that the high adhesion properties of the PAN/PBA fibrous mats for water resulted from hydrogen bonding caused by OH group of PAN/PBA fibrous mats.

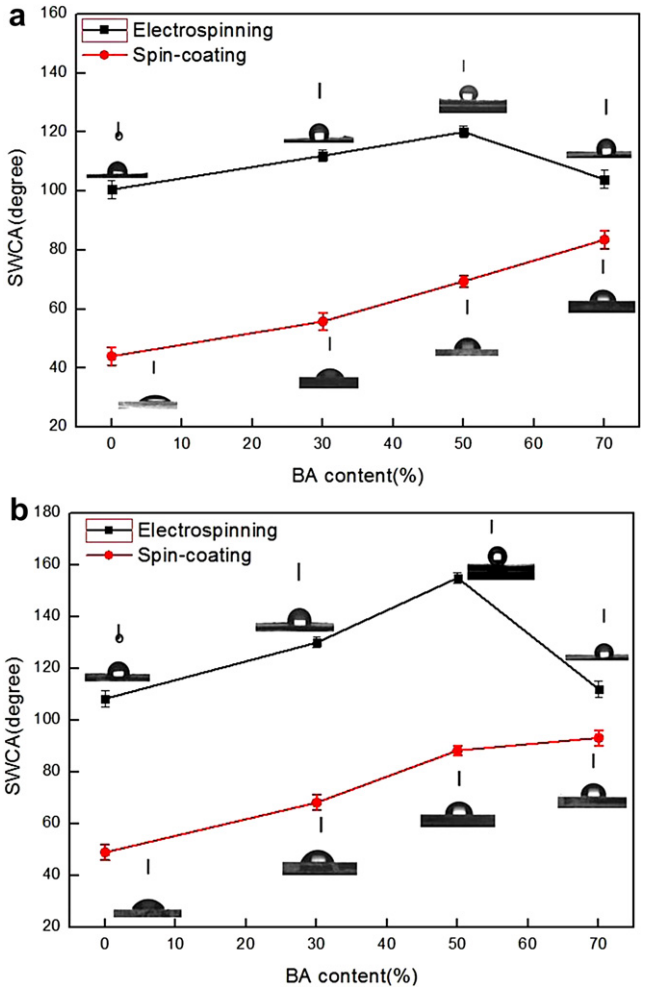


**Fig. 7.** Dependence of SWCA of (a) PAN/BA hybrids and (b) PAN/PBA blends prepared by spin-coating and electrospinning on the surface upon increase of BA content.

In general, zwitterionic polymers, including poly(-phosphorylcholine) (PPC), poly(sulfobetaine methacrylate) (PSBMA) and poly(carboxybetaine methacrylate) (PCBMA), etc., are a kind of biomimetic materials, in which cation and anion groups

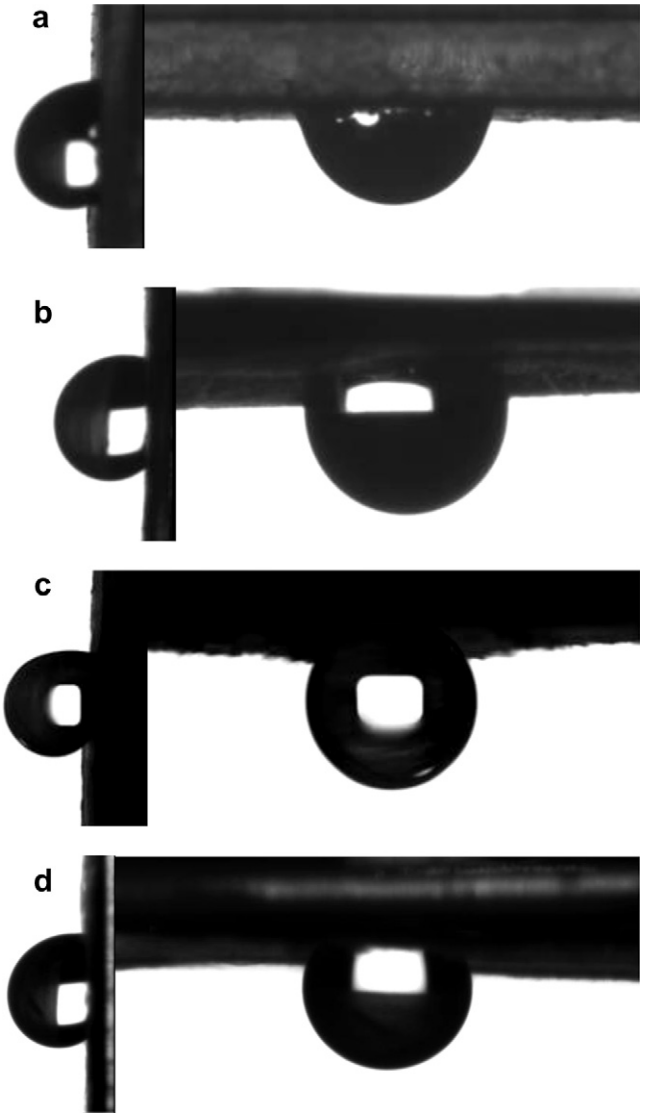


**Fig. 8.** Shapes of a water droplet on the electrospun PAN/PBA hybrid fiber surface with different tilt angles: 90° (left) and 180° (right) for (a) P10PB0, (b) P7PB3, (c) P5PB5, and (d) P3PB7, respectively.

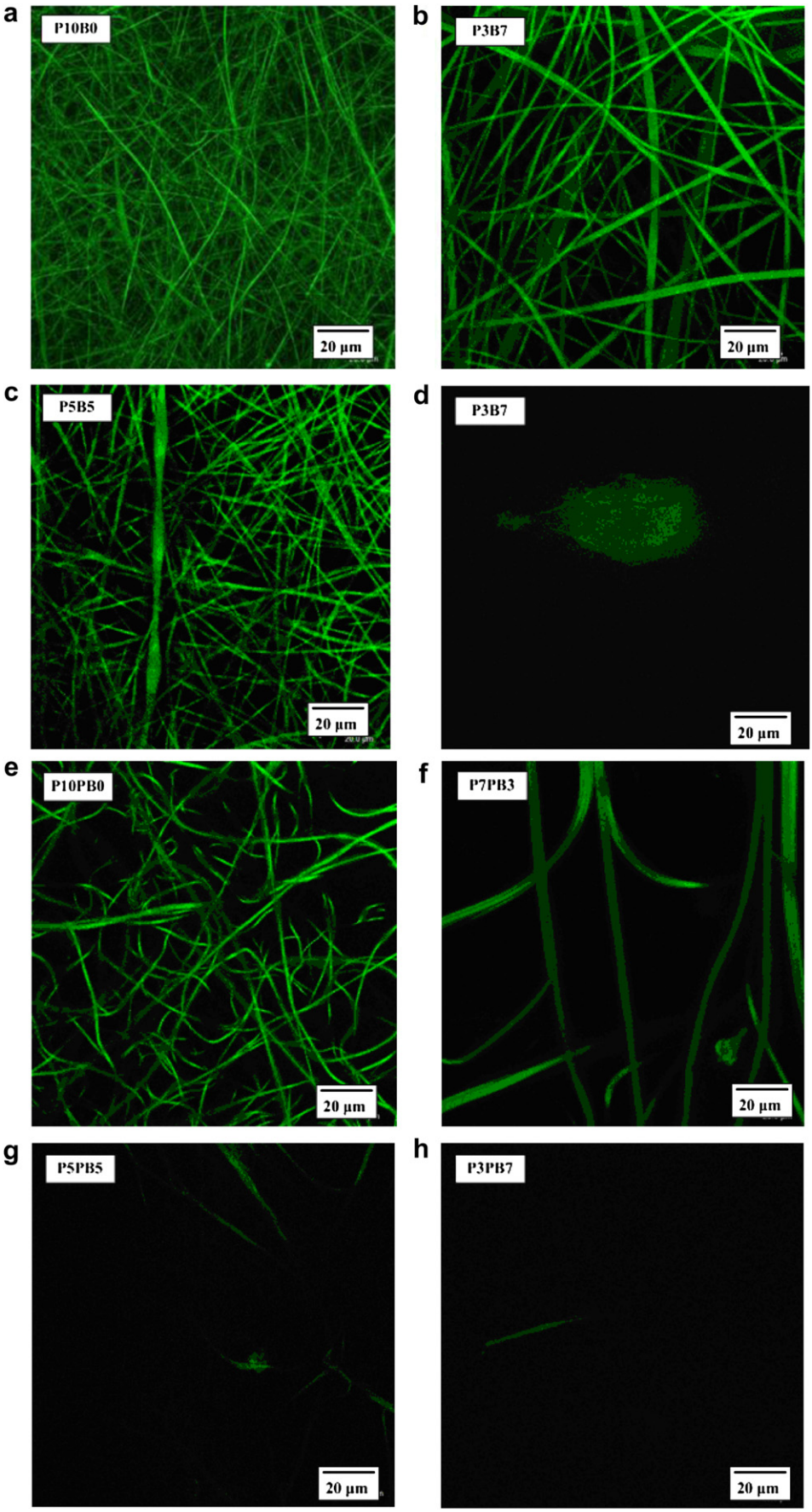


**Fig. 9.** Confocal images after fibers immersed in FTIC-conjugated antibody for 12 h: (a) P10B0, (b) P7B3, (c) P5B5, (d) P3B7, (e) P10PB0, (f) P3PB7, (g) P5PB5 and (h) P3PB7 fiber mats.

are located on the same monomer residue and maintain an overall charge neutrality [39]. Because of the strong capacity to form a hydration layer via electrostatic interaction between zwitterions and water molecules, zwitterionic polymers are recognized as unique type of materials that have excellent nonfouling properties [40]. The strategy of using low-surface-free-energy polymers without fluorine and silicon to enhance the nonfouling performance of various separation membranes has not drawn great attention recently. Most of the studies have only focused on the antiprotein adsorption property of the zwitterionic polymer modified membranes, and very few attempts have been made to examine the nonfouling performance of low-surface-free-energy polymers [41]. FTIC-conjugated antibodies were used as the probe proteins to evaluate their effects on the non-biofouling performance of the prepared fibers. Fig. 9a–d show the LSCM images of the various PAN/BA hybrid fibers after immersion in FTIC-conjugated antibodies for 12 h. It can be seen that most of the antibodies adhering on the original PAN fiber surface are viable (Fig. 9a), while those on the PAN/BA fiber surfaces (Fig. 9b, c) are less slightly upon increase of the BA to 50 wt%. The antibody absorption on the surfaces of the original PAN fiber is certainly undesirable for membrane separation. For P3B7, only few areas adhering antibodies are observed by LSCM without apparent fiber structure, in good agreement with the SEM observation (Fig. 9d). After curing the PAN/BA hybrid fibers, the surface free energy of these fiber mats had been reduced abruptly to be non-biofouling membranes as shown in Fig. 9e–h. It was found that the original PAN fibers were also highly susceptible to protein adsorption (Fig. 9e). Comparing with the PAN/BA hybrid fibers, it can be seen that amount of antibodies on the PAN/PBA blend fiber surfaces reduces apparently upon increase of the PBA content to 50 wt% (Fig. 9f, g). Most of the FTIC-conjugated antibodies adhered solely on the fibers possessing diameter in the range of 3–5 μm for P7PB3 and P5PB5 because of their larger contact area with the antibodies. Most of the blend fibers below 500 nm of fiber diameter exhibit excellent non-biofouling performance. For P3PB7, the antibody mostly vanished (Fig. 9h); even it has the largest contact area of dripping with the antibodies. When PAN blended with PBA, the non-biofouling properties of the fibers show a strong dependence on the surface free energy of the fibers. Blending PBA into PAN as electrospun fibers could effectively resist antibody adsorption. It is well known that, driven by thermodynamic forces, the low-surface-free-energy component(s) likes to segregate to the fibers to minimize the total surface free energy of the blend fibers. The LSCM studies clearly demonstrate that blending sufficient PBA into PAN can significantly change the surface free energy of fibers, improving protein adsorption resistance.

## 4. Conclusions

This study demonstrates that BA hybridizes with PAN is a thermodynamically favorable process that can be explored for preparing low surface energy PAN/PBA blend fibers without fluorine and silicon by electrospinning, depending on the initial amount of BA. We explore a non-covalent interaction between PAN and PBA by use of intermolecular hydrogen bonding. These blends comprising intermolecular hydrogen bonding could introduce the low surface energy polymer, PBA, to solidify as a fibrous mat without fluorine and silicon by electrospinning. The blend fibers consisting of 50 wt% PBA content exhibit both the SWCA as high as 154 ± 2° and strong adhesion to water. We suggest that this unusual adhesion phenomenon would be mainly derived from the hydrogen bonding between water and the molded surface composed of the densely-packed PAN/PBA fibers. In addition, PBA physically cross-links the PAN chains due to extensive hydrogen bonding between the species and displaces water from the polymeric network, leading to suppress the biofouling. The study demonstrates a relatively simple and yet versatile approach to electrospin fibers from low-surface-free-energy monomers, which provides the flexibility of making fiber mats without fluorine and silicon to best meet the superhydrophobicity and non-biofouling needs in applications. Therefore, it is feasible to develop optimized fibers by blending a low-surface-free-energy polymer into a base polymer matrix for electrospinning.

## Acknowledgments

We thank the National Science Council of the Republic of China for supporting this research financially.

## References

[1] Zhao H, Law KY. Langmuir 2012;28(32):11821–7.
[2] Jin M, Feng X, Feng L, Sun T, Zhai J, Li T, et al. Adv Mater 2005;17:1977.
[3] Hong X, Gao X, Jiang L. J Am Chem Soc 2007;129:1478.
[4] Yao Y, Dong X, Hong S, Ge H, Han CC. Macromol Rapid Commun 2006;27:1627.
[5] Kamegawa T, Shimizu Y, Yamashita H. Adv Mater 2012;24(27):3697–700.
[6] Crick CR, Bear JC, Kafizas A1, Parkin IP. Adv Mater 2012;24(26):3505–8.
[7] Chen L, Yang G, Wang ST. Small 2012;8(7):962–5.
[8] Weibel DE, Michels AF, Feil AF, Amaral L, Teixeira SR, Horowitz F. J Phys Chem C 2010;114(31):13219–25.
[9] Ma W, Wu H, Higaki Y, Otsuka H, Takahara A. Chem Commun 2012;48(54):6824–6.
[10] Ma M, Hill RM, Lowery JL, Fridrikh SV, Rutledge GC. Langmuir 2005;21:5549–54.
[11] Givens SR, Gardner KH, Rabolt JF, Chase DB. Macromolecules 2007;40:608–10.
[12] McCann JT, Marquez M, Xia Y. J Am Chem Soc 2006;128:1436–7.
[13] Dalton PD, Klinkhammer K, Salber J, Klee D, Möller M. Biomacromolecules 2006;7:686–90.
[14] Grimm S, Giesa R, Sklarek K, Langner A, Gosele U, Schmidt HW, et al. Nano Lett 2008;8:1954–9.
[15] Grignard B, Vaillant A, Coninck J, Piens M, Jonas AM, Detrembleur C, et al. Langmuir 2011;27:335–42.
[16] Singh A, Steely L, Allcock HR. Langmuir 2005;21:11604–7.
[17] Han Daewoo, Steckl Andrew J. Langmuir 2009;25:9454–62.
[18] Hardman SJ, Muhamad-Sarih N, Riggs HJ, Thompson RL, Rigby J, Bergius WNA, et al. Macromolecules 2011;44(16):6461–70.
[19] Wang C, Su Yi, Kuo S, Huang C, Sheen Y, Chang F. Angew Chem Int Ed 2006;45:2248–51.
[20] Liao CS, Wu JS, Wang CF, Chang FC. Macromol Rapid Commun 2008;29:52–6.
[21] Liao CS, Wang CF, Lin HC, Chou HY, Chang FC. Langmuir 2009;25:3359–62.
[22] Kim FS, Ren G, Jenekhe SA. Chem Mater 2011;23:682–732.
[23] Agag T, Takeichi T. Macromolecules 2003;36:6010–7.
[24] Gao LC, McCarthy TJ. Langmuir 2006;22:6234–7.
[25] Wenzel RN. Ind Eng Chem 1936;28:988–94.
[26] Cassie ABD, Baxter S. Trans Faraday Soc 1944;40:546–51.
[27] Dalton S, Heatley F, Budd PM. Polymer 1999;40:5531–43.
[28] Houtz RC. Text Res J 1950;20:786–801.
[29] Grassie N, McGuchan R. Eur Polym J 1971;7:1357–71.
[30] Burlant WJ, Parsons JL. J Polym Sci 1956;22:249–56.
[31] LaCombe EM. J Polym Sci 1957;24:152–4.
[32] Ma M, Mao Y, Gupta M, Gleason KK, Rutledge GC. Macromolecules 2005;38:9742–8.
[33] Chen J-K, Wang J-H, Fan S-K, Chang J-Y. J Phys Chem C 2012;116:6980–92.
[34] Yoshimitsu Z, Nakajima A, Watanabe T, Hashimoto K. Langmuir 2002;18:5818–22.
[35] Öner D, McCarthy TJ. Langmuir 2000;16:7777–83.
[36] Bargeman D. J Colloid Interface Sci 1972;40:344–8.
[37] Geim AK, Dubonos SV, Grigorieva IV, Novoselov KS, Zhukov AA, Shapoval SY. Nat Mater 2003;2:461–3.
[38] Cho WK, Choi IS. Adv Funct Mater 2008;18:1089–96.
[39] Lowe AB, McCormick CL. Chem Rev 2002;102:4177–90.
[40] Cheng G, Zhang Z, Chen S, Bryers JD, Jiang S. Biomaterials 2007;28:4192–9.
[41] Shi Q, Ye S, Kristalyn C, Su Y, Jiang Z, Chen Z. Langmuir 2008;24:7939–46.